RSC Advances

This is an *Accepted Manuscript*, which has been through the Royal Society of Chemistry peer review process and has been accepted for publication.

Accepted Manuscripts are published online shortly after acceptance, before technical editing, formatting and proof reading. Using this free service, authors can make their results available to the community, in citable form, before we publish the edited article. This *Accepted Manuscript* will be replaced by the edited, formatted and paginated article as soon as this is available.

You can find more information about *Accepted Manuscripts* in the Information for Authors.

Please note that technical editing may introduce minor changes to the text and/or graphics, which may alter content. The journal's standard Terms & Conditions and the Ethical guidelines still apply. In no event shall the Royal Society of Chemistry be held responsible for any errors or omissions in this *Accepted Manuscript* or any consequences arising from the use of any information it contains.

ROYAL SOCIETY OF CHEMISTRY

www.rsc.org/advances

Synthesis of mono-dispersed mesoporous SBA-1 nanoparticles with tunable pore size and their application in lysozyme immobilization

Jianxiong Xu,[a,c] Weiwei Liu,[a] Yunfei Yu,[a] Jingjing Du,[a,c] Na Li[a,b,c]* and Lijian Xu[a,c]*

[a]*Hunan Key Laboratory of Green Packaging & Application of Biological Nanotechnology, Hunan University of Technology, Zhuzhou 412007, People's Republic of China*

[b]*College of Metallurgy Engineering, Hunan University of Technology, Zhuzhou 412007, People's Republic of China*

[c]*Economical Forest Cultivation and Utilization of 2011 Collaborative Innovation Center in Hunan Province, Central South University of Forest and Technology, Changsha 410004, People's Republic of China*

*Corresponding Authors: lina6980955@163.com

RSC Advances Accepted Manuscript

Abstract: One simple route synthesis of mesoporous silica nanoparticles with cubic $Pm\bar{3}n$ pore structure (SBA-1) and controlled pore size is reported. The synthesis of mesoporous silica nanoparticles is achieved by employing organic mesomorphous complexes of polyelectrolyte (poly(acrylic acid)) and cationic surfactant (hexadecyl pyridinium chloride) as template, and tetrapropoxysilane as silica source. It is found that the pore size of the synthesized mesoporous silica nanoparticles can be tuned by the incorporation of 1,3,5-trimethylbenzene. By adjusting the amount of 1,3,5-trimethylbenzene in the synthesis, a series of silica nanoparticles with controlled pore size ranging from 2.5 nm to 5.3 nm are obtained. The adsorption properties of the mesoporous silica nanoparticles with different pore size against lysozyme are compared. The results show that mesoporous silica nanoparticles with proper pore size and well ordered pore structure benefit to the adsorption and exhibit low leaching rate.

Keywords: Mesoporous silica nanoparticles; 1,3,5-Trimethylbenzene; Lysozyme; Adsorption

RSC Advances Accepted Manuscript

1. Introduction

The development of modern biotechnology as well as its expanding applications has much to offer with respect to green and sustainable chemistry in various fields such as pharmaceuticals, fine-chemical syntheses, biosensing, proteome analyses and biofuel cells.[1] The utilization of enzymes as biocatalysts has become an important avenue in chemical and pharmaceutical industries to prepare biochemical products, biosensors and drugs.[2-5] Compared to traditional (chemical) catalysts, the use of enzymes generally is more environmentally friendly and economic due to low energy cost, high efficiency, high chemo-, regio-, and stereo-selectivities and shorter synthetic routes.[6-8] However, most of native enzymes exhibit high reactivity and selectivity only under normal conditions. Under extreme temperatures or pH, enzymes are easily inactivated due to denaturation, either by changes of conformation or other transformations of stereo chemical structure.[9] During the past few decades, immobilization of enzymes on solid materials has been widespread interest due to the advantages of immobilized enzymes with respect to enhanced stability, repeated use, facile separation from reaction mixtures, and the prevention of enzyme contamination in products.[10-15] Up to now, both inorganic and organic materials, such as porous glass,[16] cellulose,[17] chitosan,[18] polymer,[19] and mesoporous silica[20-24] are often used as supports for enzyme immobilization.

Recently, mesoporous silica nanoparticles have received much attention as promising host materials for guest biomolecules such as enzyme and protein because of their uniform pore size, open pore structure, large surface area as well as chemical

RSC Advances Accepted Manuscript

and mechanical stabilities.[25] It has been found that two factors may greatly influence the immobilization behavior of mesoporous silica nanoparticles. One is the structure and morphology. Materials like MCM-41,[26] FSM-16,[27] and SBA-15[28] have one-dimensional pore structure, where diffusion of the enzyme into the core of the particle may be limited due to pore blocking at the pore mouth. In contrast, materials possess three-dimensional interconnected pore structure, which should reduce potential diffusion limitations, may be of greatly useful in enzyme immobilization.[29] Up to now, several mesoporous silica nanoparticles with 3-D pore systems such as SBA-1,[30,31] FDU-12,[32] MCM-48[33] and SBA-16[34] have been reported and used as scaffold for enzyme immobilization. Among of them, mesoporous silica SBA-1 is an interesting material which possesses cage-type structure with 3-D interconnected small open windows.[35] This makes SBA-1 the promising candidate for enzyme immobilization. The general synthesis route for SBA-1 is based on the $S^+X^-I^+$ pathway, where S, X, and I correspond to surfactant, halide, and inorganic species, respectively, under highly acidic conditions by using surfactants with large headgroups, for example, cetyltrimethylammonium bromide (CTAB), as the templating agent.[36-39] However, the reported SBA-1 materials often have large particle sizes (micrometer or sub-micrometer) which caused a relative small surface area and lead to low loading amounts when they are used as supports for enzyme immobilization.[36,38] What's more, the SBA-1 materials synthesized under acidic condition have poor stability due to the low cross-linking degree.[39] This will greatly limit their application in enzyme immobilization. Although great efforts have been made, basic condition synthesis of

RSC Advances Accepted Manuscript

SBA-1 with good long-range structural ordering and high stability is still a challenging objective. The other factor is the pore size. Particles with small pore size are not suitable for enzymes immobilization since most of the enzymes are adsorbed on the surface of particles. A relative large pore size favors enzyme loading but leads to an increase in enzyme desorption from particles when they are re-dispersed in solution.[40] In the general synthesis of SBA-1, the pores are originated from the cationic cetyltrimethylammonium surfactant micelles owing to their strong association with silica precursors. Thus, the pore size of SBA-1 has been mostly limited to around 3 nm. On the other hand, the application of SBA-1 as scaffold for enzymes immobilization requires uniform pore sizes in the range of 4–8 nm.[41] Therefore, the synthesis of SBA-1 nanoparticles (particle size below 200 nm) with controlled pore size is highly desired in the enzymes immobilization.

Herein, we reported the facile synthesis of mono-dispersed SBA-1 nanoparticles with cubic $Pm\bar{3}n$ pore structure by employing the organic mesomorphous complexes of polyelectrolyte (poly(acrylic acid) (PAA)) and cationic surfactant (hexadecyl pyridinium chloride (CPC)) as template, and tetrapropoxysilane (TPOS) as silica source under basic condition. By using 1,3,5-trimethylbenzene as pore-expanding agent, the mesopore size of the SBA-1 nanoparticles could be tuned from 2.5 nm to 5.3 nm. Moreover, the adsorption abilities of the synthesized SBA-1 nanoparticles against lysozyme were evaluated.

2. Experimental

2.1 Materials

RSC Advances Accepted Manuscript

Hexadecyl pyridinium chloride (CPC), 1,3,5-trimethylbenzene (TMB) and tetrapropoxysilane (TPOS) were obtained from Aladdin, China. Poly(acrylic acid) (PAA) (average molecular weight=240000 g/mol, 25% solution in water) was obtained from Acros. In this work, the amount of PAA used in the synthesis means the weight of the 25% solution. Lysozyme and Micrococcus lysodeikticus cells were obtained from Sigma-Aldrich. All the chemical reagents were used without further purification.

2.2 Synthesis

2.2.1 Synthesis of SBA-1 Nanoparticles

In a typical synthesis, 0.11 g of CPC and 0.7 g of PAA solution were dissolved in 100 mL of deionized water under stirring, followed by the introduction of 0.8 g of ammonia solution (25%). After further stirring for 20 min, 0.53 g of TPOS was added. The mixture was stirred for 30 min, and then transferred to an autoclave at 80 ^{o}C for 48 h. The final product was centrifugated, washed with deionized water, and dried at 60 ^{o}C. The organic template was removed by calcination at 550 ^{o}C for 5 h.

2.2.2 Incorporation of 1,3,5-TMB as pore-swelling agents

The incorporation of 1,3,5-TMB as pore-swelling agent was carried out using procedure similar to that described above. After the addition of ammonia solution, different amounts of 1,3,5-TMB was subsequently added and stirred for 30 min. Then, 0.53 g of TPOS was added dropwisely into the above solution. After being stirred for 30 min, the mixture was put in an oven of 80 ^{o}C for 48 h. The final product was centrifugated, washed, dried and calcined at 550 ^{o}C for 5 h. The samples were denoted

RSC Advances Accepted Manuscript

as SBA-1-x (Where the suffix number x indicates the amount of TMB used in the synthesis).

2.3 Lysozyme Immobilization

Approximately 5 mg of the silica sample was dispersed in 10 mL of lysozyme stock solution with initial concentration ranging from 0.1 ~ 1.0 mg mL^{-1} in phosphate buffer solution (PBS, 50 mM, pH = 7.0). The suspensions were continuously shaken for 24 h at 25 ^{o}C and then separated by centrifugation at 12000 rpm for 5 min. The resultant lysozyme immobilized SBA-1 pellets were washed twice with 5 mL of phosphate buffer solution. The supernatants of the lysozyme solution were collected and combined. Lysozyme concentrations were determined using the characteristic ultraviolet-visible light (UV-vis) absorbance of lysozyme at 280 nm. The difference in the lysozyme amount in solution before and after adsorption was deemed equal to the amount of lysozyme adsorbed on the material.

2.4 Stability/Leaching Studies

The samples of lysozyme immobilized SBA-1 nanoparticles were examined by desorption experiments in aqueous solution under the magnetic agitation. In the case of a normal desorption, the lysozyme immobilized particles (5 mg) were redispersed in 10 mL of fresh phosphate buffer solution (pH = 7.0), and then equilibrated for a desirable time (about 12 h) to ensure a steady state, prior to centrifugation. After that, the supports were rinsed three times with 5 mL of phosphate buffer solution. The concentration of the desorbed lysozyme in the supernatant was determined by UV-vis. The rate of leaching was then obtained through the formulation of the amount of

RSC Advances Accepted Manuscript

desorption divided by the total amount of lysozyme loaded.

2.5 Enzymatic Activity

The activity of both free lysozyme and immobilized lysozyme was assayed by a standard method using Micrococcus cells.[42] The lysozyme-silica composites were suspended in phosphate buffer (50 mM) at pH 6.2 for 2 h before reaction. The Micrococcus lysodeikticus solution was prepared by dissolving 9 mg of Micrococcus lysodeikticus in 25 mL phosphate buffer. Then, in a vial, 5 mL of free or immobilized lysozyme solutions/dispersion (all samples set to be 100 μg enzyme/mL) were mixed with 5 mL of Micrococcus lysodeikticus solution. After stirring for 5 min, 1.5 mL of the reacted solution was centrifuged at 4 °C (for quenching the reaction), and the supernatants were taken to measure UV absorbance at 450 nm by a UV spectrometer. The difference of UV absorbance at 450 nm was recorded to calculate the activity.

2.5 Characterization

The X-ray diffraction (XRD) patterns were obtained on a Rigaku Model D/max-2500 diffractometer, with Cu Kα radiation at 40 kV and 100 mA. SEM images were obtained with a Shimadzu SS-550 instrument. TEM observations were performed on a Philips Tecnai F20 microscope, working at 200 kV. All samples subjected to TEM measurements were dispersed in ethanol ultrasonically and were dropped on copper grids. N_2 adsorption measurements were performed on a BELSORP-mini II sorption analyzer. The specific surface area was calculated by BET (Brunauer-Emmett-Teller) method, the pore size distribution was calculated from the adsorption branch using BJH (Barett-Joyner-Halenda) method and total pore volume

RSC Advances Accepted Manuscript

was obtained at P/P_0 of 0.99. Before measurements, the samples were dried under dry N_2 flow at 350 ^oC for 5 h. Fourier Transform Infrared (FTIR) measurements were recorded using Bruker VECTOR 22 spectrometers with wavenumber precision < 0.01 cm^{-1} and signal-to-noise 30000:1. UV-vis spectra were measured on a Shimadzu Model 2450 spectrometer.

3. Results and discussion

3.1 Synthesis of SBA-1 nanoparticles

The synthesis of SBA-1 nanoparticles was achieved by employing the organic mesomorphous complexes of PAA/CPC as template, and TPOS as silica source. Figure 1A showed the XRD pattern of the calcined SBA-1 sample. The XRD pattern of the sample exhibited three well-resolved diffraction peaks, which were indexed to the (200), (210), and (211) characteristic diffractions of the cubic $Pm\bar{3}n$ mesostructure of SBA-1. The morphology and interior structure of the SBA-1 nanoparticles were characterized by SEM and TEM. The SEM image (Figure 2A) showed that the SBA-1 nanoparticles had a uniform pore size distribution, and the average diameter was 90 nm. In the high-resolution TEM images (Figure 2B, C), the mesopores of the SBA-1 mesostructure could be observed and within the entire sphere, the alignment of mesopores kept well long-range order. From Figure 2D, the typical [100] direction of the SBA-1 was clearly observed indicating the cage-type pore structure of SBA-1 nanoparticles. The nitrogen adsorption-desorption isotherm and the pore size distribution curve of the SBA-1 nanoparticles were shown in Figure 1B. The isotherm was type IV with a type-H_2 hysteresis loop at relative pressure (P/P_0) of

RSC Advances Accepted Manuscript

0.3-0.6, which corresponded to nitrogen capillary condensation in the cagelike mesopores of SBA-1. The BET surface area and the pore volume of SBA-1 nanoparticles were 355 m^2/g and 0.80 cm^3/g, respectively, as summarized in Table 1. According to the Barrett-Joyner-Halenda (BJH) method, the average pore size was calculated to be 2.5 nm as shown in the pore size distribution curve (the inset of Figure 1B). The adsorption step at P/P_0 of 0.9-0.99 resulted in a broad pore size distribution centered at about 100 nm, which could be attributed to the voids between nanoparticles.

It was worthy noting that the synthesized SBA-1 nanoparticles containing one type of mesopore. However, in our previous study we reported the synthesis of hierarchically porous SBA-1 nanoparticles by employing the organic mesomorphous complexes of PAA/CPC as template, and tetraethoxysilane (TEOS) as silica source.[35] Hierarchically porous SBA-1 nanoparticles were formed through a "dynamic template" mechanism, where the CPC micelles acted as mesoporous template while the phase separated PAA chains acted as the secondary nanoporous template. The main difference of the two systems involved the utilization of different silica source. Compared with TEOS, TPOS has a slower hydrolysis rate.[43] During the hydrolysis of TPOS, the generated negatively charged silica oligomers slowly penetrated into the mesomorphous PAA/CPC complexes owing to their strong association of CPC surfactant with silica oligomers. The electrostatic repulsive force between the inorganic species and PAA chains made the peeling of the PAA chains from PAA/CPC complexes. The peeled PAA chains would diffuse into the water phase. Since the

RSC Advances Accepted Manuscript

TPOS had a slowly hydrolysis and concentration rate, before the morphology fixing of the SBA-1 nanoparticles the PAA chains were totally peeled off from the PAA/CPC complexes and diffused into the water phase. This meant that only the cationic CPC surfactant micelles were acted as the pore-forming agent and therefore the synthesized SBA-1 nanoparticles containing one type of mesopore as illustrated in Scheme 1. To demonstrate the existence of PAA chains in the water phase, a confirmatory experiment was made. After the centrifugation of the as-synthesized SBA-1 nanoparticle colloids dispersion, the supernatant was concentrated and precipitated in acetone, obvious white flocculent precipitates were observed. This further demonstrated that during the formation of SBA-1 nanoparticles the PAA chains were peeled off from the PAA/CPC complexes and existed in the water phase. The morphology of the synthesized SBA-1 nanoparticles was originated from the PAA/CPC complexes since amorphous mesoporous silicas were obtained if only CPC surfactant was used as template, as shown in Figure S1.

3.2 Pore expanding of SBA-1 nanoparticles

It is well known that the pore size of mesoporous silica nanoparticles is a key parameter in enzyme immobilization.[44] Mesoporous silica nanoparticles with a proper pore size might lead to high immobilization efficiency and decrease the likelihood of enzyme desorption from particles when they were redispersed in solution. Therefore, the control of pore size of mesoporous silica nanoparticles was highly important in designing scaffold for enzyme immobilization. The incorporation of alkanes as swelling agents was an effective method to control the pore size of mesoporous

RSC Advances Accepted Manuscript

silica.[40] Herein, to expand the size of the ordered mesopore of SBA-1 nanoparticles, 1,3,5-trimethylbenzene (TMB) was used as an organic swelling agent in the synthesis. The XRD patterns of the calcined products synthesized with different amounts of 1,3,5-TMB were shown in Figure 3 (curve b~d). It was found that with the addition of 1,3,5-TMB, the originally resolved peaks (Figure 3, curve a) broadened and merged together. The broad peak shifted to lower angle with increasing the amount of 1,3,5-TMB indicating the degraded long-range order of the mesostructure and the increase of the *d*-spacing.[42] The N_2 adsorption-desorption isotherms and pore size distribution curves of the samples synthesized with different amount of 1,3,5-TMB were shown in Figure 4. It was observed that the size of the cagelike mesopore of SBA-1 was gradually increased from 2.5 nm to 5.3 nm, and BET surface area were increased from 355 m^2/g to 798 m^2/g with the addition of 1,3,5-TMB (see Table 1).

The TEM images of the calcined SBA-1 synthesized with different amount of 1,3,5-TMB were shown in Figure 5. As shown in Figure 5, the morphology of the synthesized SBA-1 samples with the addition of 1,3,5-TMB remained almost unchanged, whereas, the particle size gradually increased from 100 nm to 130 nm with the amount of 1,3,5-TMB increased from 0.08 g to 0.45 g. Moreover, the pore size of the SBA-1 nanoparticles became more pronounced and the alignment of the mesopores still maintained good long-range order within the particle with the amount of 1,3,5-TMB below 0.30 g. These results suggested that the addition of 1,3,5-TMB not only swelled the surfactant micelles to enlarge the mesopores, but also swelled the PAA/CPC complexes to enlarge the particle size of SBA-1.

RSC Advances Accepted Manuscript

3.3 Immobilization of lysozyme on SBA-1 nanoparticles

In order to highlight the improved properties of the pore-expanded SBA-1 nanoparticles, the synthesized SBA-1 nanoparticles with different pore size were used as scaffold for lysozyme (dimensions: 4.5 × 3.0 × 3.0 nm^3) immobilization. These experiments were performed at pH = 7.0 which was below the isoelectric point of lysozyme (pI = 11) and well above the isoelectric point of SiO_2 (pI = 2). Hence, electrostatic interaction between the positively charged lysozyme and the negatively charged SBA-1 nanoparticles should be the main driving force of adsorption. The adsorption isotherms of lysozyme loaded onto SBA-1 nanoparticle supports with different pore size were shown in Figure 6A. The general trend was increase in the adsorption capacity with the increase in initial lysozyme concentration. For the SBA-1, SBA-1-0.08, SBA-1-0.3, and SBA-1-0.45 nanoparticles, with increasing the initial lysozyme concentration from 0.1 ~ 1.0 mg mL^{-1} the adsorption amount increased from 55 to 195 mg/g, 88 to 266 mg/g, 104 to 298 mg/g, and 134 to 324 mg/g, respectively. Compared with original SBA-1 nanoparticle, the pore expanded SBA-1 nanoparticles offered higher lysozyme loading. For example, under the adsorption condition of initial lysozyme concentration at 0.5 mg mL^{-1}, the adsorption amount for SBA-1, SBA-1-0.08, SBA-1-0.3, and SBA-1-0.45 nanoparticles were 165 mg/g, 229 mg/g, 268 mg/g and 297 mg/g, respectively. Since the pore diameter of SBA-1 nanoparticles was 2.5 nm which was smaller than the size of lysozyme molecules, lysozyme should in principle only be adsorbed on the external surface of SBA-1 nanoparticles. However, for the pore expanded SBA-1-0.08, SBA-1-0.30 and

RSC Advances Accepted Manuscript

SBA-1-0.45 nanoparticles, the pore size were 3.8 nm, 4.8 nm and 5.3 nm, respectively, which were more comfortable for lysozyme immobilization and resulted in higher lysozyme loading.

To quantify the adsorption capacity and the strength of the lysozyme/silica interaction, we have used the well-known Langmuir equation:

$$\frac{C_e}{q_e} = \frac{1}{q_{max} K_L} + \frac{C_e}{q_{max}}$$

where C_e (mg/mL) was the equilibrium concentration of lysozyme, q_e (mg/g) was the adsorption capacity at a certain time, q_{max} (mg/g) was the maximal loading of lysozyme, and K_L (mL/g) was Langmuir constant related to the binding sites affinity respectively.[40] Linearized plots of C_e/q_e versus C_e was obtained from the model, as shown in Figure 6B, demonstrating that all the adsorption isotherms fitted the Langmuir model. Based on the slope and interception of the linearized plots, the q_{max} and K_L were calculated and the results were summarized in Table 1. As shown, the q_{max} of lysozyme on SBA-1, SBA-1-0.08, SBA-1-0.30 and SBA-1-0.45 nanoparticles were 250 mg/g, 346 mg/g, 391 mg/g and 409 mg/g, respectively. That is, larger the mesopore of SBA-1 nanoparticles, higher the adsorption amount. This might be due to the improved surface area and the expanded pore size, which led to the good accessibility to the pores, and low mass-transfer resistance.

3.4 Leaching Investigation

For enzyme immobilization via the adsorption or encapsulation approach, the leakage of enzyme was usually a big accompanied problem and disadvantage.[45] Here we took the lysozyme immobilized particles prepared under the condition that initial

RSC Advances Accepted Manuscript

lysozyme concentration at 0.5 mg mL^{-1}, adsorption time of 24 h, adsorption temperature at 25 ^{o}C as typical examples. Figure 7 showed the leaching of lysozyme increased along with time. For all the leaching profiles, a relatively fast desorption was observed within the first 8 h. After then, since some of the desorbed lysozyme could be re-absorbed onto the matrixes, the absorption rate would drop slightly. More importantly, the leaching property also showed the pore size dependence. The lysozyme immobilized on SBA-1-0.30 nanoparticles achieved a lower desorption rate (about 4.6%) of lysozyme after 8 h. This might be mainly ascribed to their proper pore size and well ordered pore structure, which would effectively grip the lysozyme. In contrast, a higher desorption-rate (about 10 %) of lysozyme was observed after 8 h by using the SBA-1 nanoparticles since the lysozyme should mainly adsorbed on the external surface of SBA-1 nanoparticles. Compared with the SBA-1-0.30 nanoparticles, the desorption-rate of lysozyme on SBA-1-0.08 (about 7.6 %) and SBA-1-0.45 (about 7.4 %) nanoparticles was higher. For the SBA-1-0.08 nanoparticles, the mesopore size was about the size of lysozyme. Thus, more lysozyme molecules could not totally be entraped into the channel of the mesopore, which resulted in a higher desorption-rate. While for the SBA-1-0.45 nanoparticles, the mesopore size was appropriate for the immobilization of lysozyme. However, the less ordered pore structure of SBA-1-0.45 nanoparticles could not effectively grip the lysozyme in the pore channel and led to in a higher desorption-rate. Based the results above, it is conclude that the relative large pore size and ordered pore structure of the synthesized SBA-1 nanoparticles was more efficient to suppress the enzyme leakage,

RSC Advances Accepted Manuscript

resulting in a more stable system.

3.5 Enzymatic Activity

In the general immobilization of enzyme, the checking of whether the enzyme denatured during the interaction with the silica matrix was indispensable. On the basis of earlier report, the amide linkages between amino acid residues in polypeptides and protein give the well-known fingerprints from the FTIR spectrum. The positions of the amide I and II bands in the FTIR spectra of proteins are sensitive indicators of conformational changes in the protein secondary structure and have been used in the study to investigate the immobilized enzymes molecules.[46] Here we took the SBA-1-0.30 nanopartiucles as a typical example. Figure 8 showed the FTIR spectra of the pure lysozyme (a), the SBA-1-0.30 scaffold (b) and lysozyme-immobilized SBA-1-0.30 nanopartiucles (c). The inset of Figure 7 represented the magnified FTIR spectra at the wavenumber region of 1800 cm^{-1} ~ 1300 cm^{-1}. As shown, the amide I peak at about 1660 cm^{-1} can be observed at lysozyme and lysozyme-immobilized silica. Additionally, the peak at 1530 cm^{-1}, corresponding to the amide II band, can also be clearly seen in lysozyme-immobilized silica. These spectral characteristics indicated that the secondary structure of the protein was maintained in the immobilized lysozyme molecules and also indicated that as-prepared silica carriers were compatible with the physiological medium.[47]

Further more, the activity of immobilized lysozyme prepared under the adsorption condition of initial lysozyme concentration at 0.5 mg mL^{-1} with different SBA-1 samples as scaffold was determined by using the free lysozyme as a control.

RSC Advances Accepted Manuscript

The results were summarized in Table 2. As shown, the enzymatic activity of the free lysozyme in solution was about 8640 U/mg. The immobilized lysozyme molecules partly lost enzymatic activities due to adsorption on silica. Besides, the activity of immobilized lysozyme decreased with the increase in the pore size of SBA-1 scaffold. Lysozyme immobilized onto solid silica nanoparticles possessed the highest relative activity, which can be explained based on the fact that the lysozyme molecules were mainly adsorbed on the external surface of solid SBA-1 nanoparticles as discussed above. However, with the increasing of the SBA-1 pore size more and more lysozyme molecules were entrapped into the mesopore of SBA-1 nanoparticles. This led to less chance of lysozyme contacting the bacteria and therefore a decreased enzyme activity.[48] But the appearance of enzyme activity on SBA-1 nanoparticles indicated that the active site of lysozyme still worked. That is, the essential protein structure of lysozyme, which is necessary for it to act as an enzyme, was maintained.

4 Conclusions

With organic mesomorphous complexes of polyelectrolyte (poly(acrylic acid) (PAA)) and cationic surfactant (hexadecyl pyridinium chloride (CPC)) as template, and tetrapropoxysilane (TPOS) as silica source, monodispersed SBA-1 nanoparticles were successfully synthesized under basic condition. The synthesized SBA-1 nanoparticles have well-defined structure with cubic $Pm\bar{3}n$ pore structure. By means of pore-expanding with 1,3,5-trimethylbenzene, the mesopore size of the SBA-1 nanoparticles could be easily tuned from 2.5 nm to 5.3 nm, while the morphology of the particles was not dramatically changed. The synthesized SBA-1 nanoparticles

RSC Advances Accepted Manuscript

were used as scaffold for lysozyme immobilization. It was demonstrated that mesoporous silica nanoparticles with proper pore size and well ordered pore structure benefit to the adsorption and exhibit low leaching rate. Furthermore, the immobilized lysozyme retained enzymatic activity, which was important for their application. This kind of materials is anticipated to be a suitable carrier for the construction of biosensor, biocatalysis, separation, drug-delivery, and controlled release systems.

Electronic Supplementary Information available: Figure S1 showing the TEM images of the mesoporous silica synthesized with hexadecyl pyridinium chloride surfactant as template.

Acknowledgements

The financial support by the National Science Foundation of China (Grants No. 61001053), the National Science Foundation for Post-doctoral Scientists of China (Grants No. 2014T70774 and 2014M550421), the Natural Science Foundation of Hunan Province (Grants No. 14JJ3125), the Technology Planning Project of Hunan Province (Grants No. 2014SK2019 and 2013SK2003), and the Scientific Research Fund of Hunan Provincial Education Department (grant No. 14C0343, 14A040) is gratefully acknowledged.

References

1 Z. Zhou and Martin Hartmann, *Chem. Soc. Rev.*, 2013, **42**, 3894–3912.

2 H. E. Schoemaker, D. Mink and M. G. Wubbolts, *Science*, 2003, **299**, 1694–1697.

3 J. Rajendhran and P. Gunasekaran, *J. Biosci. Bioeng.*, 2004, **97**, 1–13.

4 M. J. E. C. van der Maarel, B. Van der Veen, J. M. C. Uitdehaag, H. Leemhuis and

RSC Advances Accepted Manuscript

L. Dijkhuizen, *J. Biotechnol.*, 2002, **94**, 137–155.

5 A. Liese and L. Hilterhaus, *Chem. Soc. Rev.*, 2013, **42**, 6236–6249.

6 T. Nagayasu, M. Miyanaga, T. Tanaka, T. Sakiyama and K. Nakanishi, *Biotechnol. Bioeng.*, 1994, **43**, 1108–1117.

7 Y. -F. Chang, and D. -F. Tai, *Tetrahedron: Asymmetry*, 2001, **12**, 177–179.

8 C. Bayon, A. Cortes, A. Aires-Trapote, C. Civera and M. J. Hernaiz, *RSC Adv.*, 2012, **4**, 2227–2238.

9 C. -H. Lee, T. -S. Lin and C. -Y. Mou, *Nano Today*, 2009, **4**, 165–179.

10 C. Ispas, I. Sokolov and S. Andreescu, *Anal. Bioanal. Chem.*, 2009, **393**, 543–554.

11 M. Hartmann and D. Jung, *J. Mater. Chem.*, 2010, **20**, 844–857.

12 Y. Deng, C. Deng, D. Qi, C. Liu, J. Liu, X. Zhang and D. Zhao, *Adv. Mater.*, 2009, **13**, 1377–1382.

13 A. Popat, S. B. Hartono, F. Stahr, J. Liu, S. Z. Qiao and G. Q. Lu, *Nanoscale*, 2011, **3**, 2801–2818.

14 M. Shakeri, and M. Shoda, *J. Mol. Catal. B Enzym.*, 2008, **54**, 42–49.

15 Y. Wang, and F. Caruso, *Chem. Mater.*, 2005, **17**, 953–961.

16 R. Muller, N. Anders, J. Titus, and D. Enke, *Talanta*, 2013, **107**, 255–262.

17 P. Sathishkumar, S. Kamala-Kannan, M. Cho, J. S. Kim, T. Hadibarata, M. R. Salim, and B. -T. Oh, *J. Mol. Catal. B Enzym.*, 2014, **100**, 111–120.

18 I. Belhaj-Ben Romdhane, Z. Ben Romdhane, M. Bouzid, A. Gargouri, and H. Belghith, *Appl. Biochem. Biotech.*, 2013, **171**, 1986–2002.

19 M. Xiong, B. Gu, J. -D. Zhang, J. -J. Xu, H. -Y. Chen, and H. Zhong, *Biosens.*

RSC Advances Accepted Manuscript

Bioelectron., 2013, **50**, 229–234.

20 J. F. Díaz, and K. J. Balkus Jr., *J. Mol. Catal. B: Enzym.*, 1996, **2**, 115–126.

21 H. H. P. Yiu, P. A. Wright and N. P. Botting, *Micropor. Mesopor. Mater.*, 2001, **44–45**, 763–768.

22 S. P. Maddala, D. Velluto, Z. Luklinska and A. C. Sullivan, *J. Mater. Chem. B*, 2014, **2**, 903–914.

23 Y. Masuda, S. Kugimiya, Y. Kawachi and K. Kato, *RSC Adv.*, 2014, **4**, 3573–3580.

24 M. Moritz, *Appl. Surf. Sci.*, 2013, **283**, 537–545.

25 S. -H. Wu, Y. Hung and C. -Y. Mou, *Chem. Commun.*, 2011, **47**, 9972–9985.

26 M. E. Gimon-Kinsel, V. L. Jimenez, L. Washmon and K. J. Balkus Jr., *Stud. Surf. Sci. Catal.*, 1998, **117**, 373–380.

27 H. Takahashi, B. Li, T. Sasaki, C. Miyazaki, T. Kajino and S. Inagaki, *Chem. Mater.*, 2000, **12**, 3301–3305.

28 D. Zhao, Q. Huo, J. Feng, B. F. Chmelka and G. D. Stucky, *J. Am. Chem. Soc.*, 1998, **120**, 6024–6036.

29 J. Aburto, Ayala, M., I. M. Bustos-Jaimes, E. C. Terres, J. M. Dominguez and E. Torres, *Micropor. Mesopor. Mater.*, 2005, **83**, 193–200.

30 J. -G. Wang, H. -J. Zhou, P. -C. Sun, D. -T. Ding and T. -H. Chen, *Chem. Mater.*, 2010, **22**, 3829–3831.

31 N. Li, J. -G. Wang, H.-J. Zhou, P.-C. Sun and T.-H. Chen, *Chem. Mater.*, 2011, **23**, 4241–4249.

32 G. X. Ma, Q. D. Zhong, X. G. Lu and T. H. Lu, *Acta Phys. -Chim. Sin.*, 2009, **25**,

RSC Advances Accepted Manuscript

2061–2067.

33 B. Zhao, B. Shi and R. Ma, *Eng. Life Sci.*, 2005, **5**, 436–441.

34 B. Nohair, P. T. H. Thao, V. T. H. Nguyen, P. Q. Tien, D. T. Phuong, L. G. Hy and S. Kaliaguine, *J. Phys. Chem. C*, 2012, **116**, 10904-10912.

35 N. Li, J. -G. Wang, H. -J. Zhou, P.-C. Sun and T.-H. Chen, *RSC Adv.*, 2012, **2**, 2229–2231.

36 S. Che, Y. Sakamoto, O. Terasaki and T. Tatsumi, *Chem. Mater.*, 2001, **13**, 2237–2239.

37 Y. -C. Pan, H.-Y. Wu, L. -P. Lee, G. -L. Jheng, G. T. K. Fey and H. -M. Kao., *Micropor. Mesopor. Mater.*, 2009, **123**, 78–90.

38 T. Suteewong, H. Sai, R. Cohen, S. Wang, M. Bradbury, B. Baird, S. M. Gruner and U. Wiesner, *J. Am. Chem. Soc.*, 2011, **133**, 172–175.

39 C. -C. Ting, H. -Y. Wu, Y. -C. Pan, S. Vetrivel, G. T. K. Fey and H. -M. Kao. *J. Phys. Chem. C*, 2010, **114**, 19322–19330.

40 S. Cao, L. Fang , Z. Zhao, Y. Ge, S. Piletsky and A. P. F. Turner, *Adv. Funct. Mater.*, 2013, **23**, 2162–2167.

41 K. -C. Kao and C. -Y. Mou, *Micropor. Mesopor. Mater.*, 2013, **169**, 7–15.

42 Y. Wu and M. A. Daeschel, *J. Food Sci.*, 2007, **72**, 369–374.

43 I. S. Paulino, *Stud. Surf. Sci. Catal.*, 2002, **141**, 93–100.

44 S. -H. Wu, C. -Y. Mou and H. -P. Lin, *Chem. Soc. Rev.*, 2013, **42**, 3862–3875.

45 U. Hanefeld , L. Gardossi and E. Magner, *Chem. Soc. Rev.*, 2009, **38** , 453–468.

46 W. Bian, L. -L. Lou, B. Yan, C. Zhang, S. Wu and S. Liu, *Micropor. Mesopor.*

RSC Advances Accepted Manuscript

Mater., 2011, **143**, 341–347.

47 Q. -G. Xiao, X. Tao, H. -K. Zou and J. -F. Chen, *Chem. Eng. J.*, l 2008, **137**, 38–44.

48 A. Kawai, Y. Urabe, T. Itoh and F. Mizukami, *Mater. Chem. Phys.*, 2010, **122**, 269–272.

RSC Advances Accepted Manuscript

Captions

Figure 1. (A) The XRD pattern and (B) nitrogen adsorption-desorption isotherm with the inset pore size distribution of the calcined SBA-1 nanoparticles.

Figure 2. The SEM (A) and TEM (B-D) images of the calcined SBA-1 nanoparticles.

Scheme 1. Schematic synthesis of SBA-1 nanoparticles employing organic mesomorphous complexes of PAA/CPC as template, and TPOS as silica source.

Figure 3. The XRD patterns of the pore-expanded SBA-1 nanoparticles prepared with different amounts of 1,3,5-TMB: SBA-1 (pattern a), SBA-1-0.08 (pattern b), SBA-1-0.30 (pattern c) and SBA-1-0.45 (pattern d).

Figure 4. (A) Nitrogen adsorption-desorption isotherms and (B) pore size distribution curves of the pore-expanded SBA-1 nanoparticles prepared with different amounts of 1,3,5-TMB: SBA-1 (curve a), SBA-1-0.08 (curve b), SBA-1-0.30 (curve c) and SBA-1-0.45 (curve d).

Figure 5. The TEM images of the pore-expanded SBA-1 nanoparticles prepared with different amounts of 1,3,5-TMB: SBA-1-0.08 (A, B), SBA-1-0.30 (C, D) and SBA-1-0.45 (E, F).

Figure 6. Adsorption isotherms after 24 h (A) and Langmuir isotherms (B) of lysozyme on SBA-1, SBA-1-0.08, SBA-1-0.30 and SBA-1-0.45, respectively.

Figure 7. Leaching profiles of lysozyme loaded on SBA-1, SBA-1-0.08, SBA-1-0.30 and SBA-1-0.45, respectively.

Figure 8. The FTIR spectra of the pure lysozyme (a), the SBA-1-0.30 scaffold (b) and lysozyme-immobilized SBA-1-0.30 nanopartiucles (c). The inset represented the

RSC Advances Accepted Manuscript

magnified FTIR spectra at the wavenumber region of 1800 cm^{-1} ~ 1300 cm^{-1}.

Table 1. Physicochemical properties of the calcined SBA-1 samples synthesized with different amount of 1,3,5-TMB.

Table 2. Activity of immobilized lysozyme prepared under the adsorption condition of initial lysozyme concentration at 0.5 mg mL^{-1} with different SBA-1 samples as scafford.

RSC Advances Accepted Manuscript

Fig. 1.

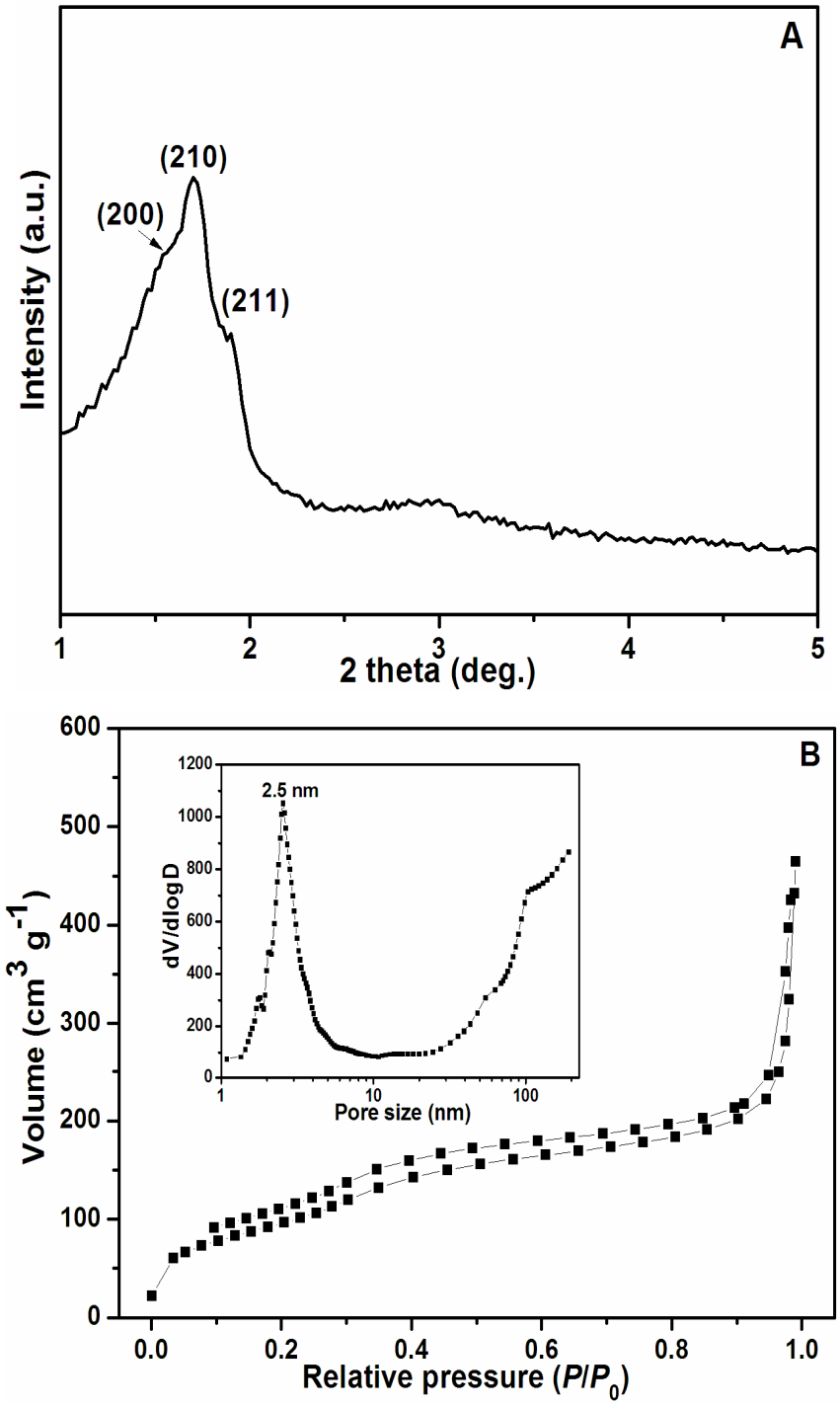

Xu, et al., Fig. 1.

RSC Advances Accepted Manuscript

Fig. 2.

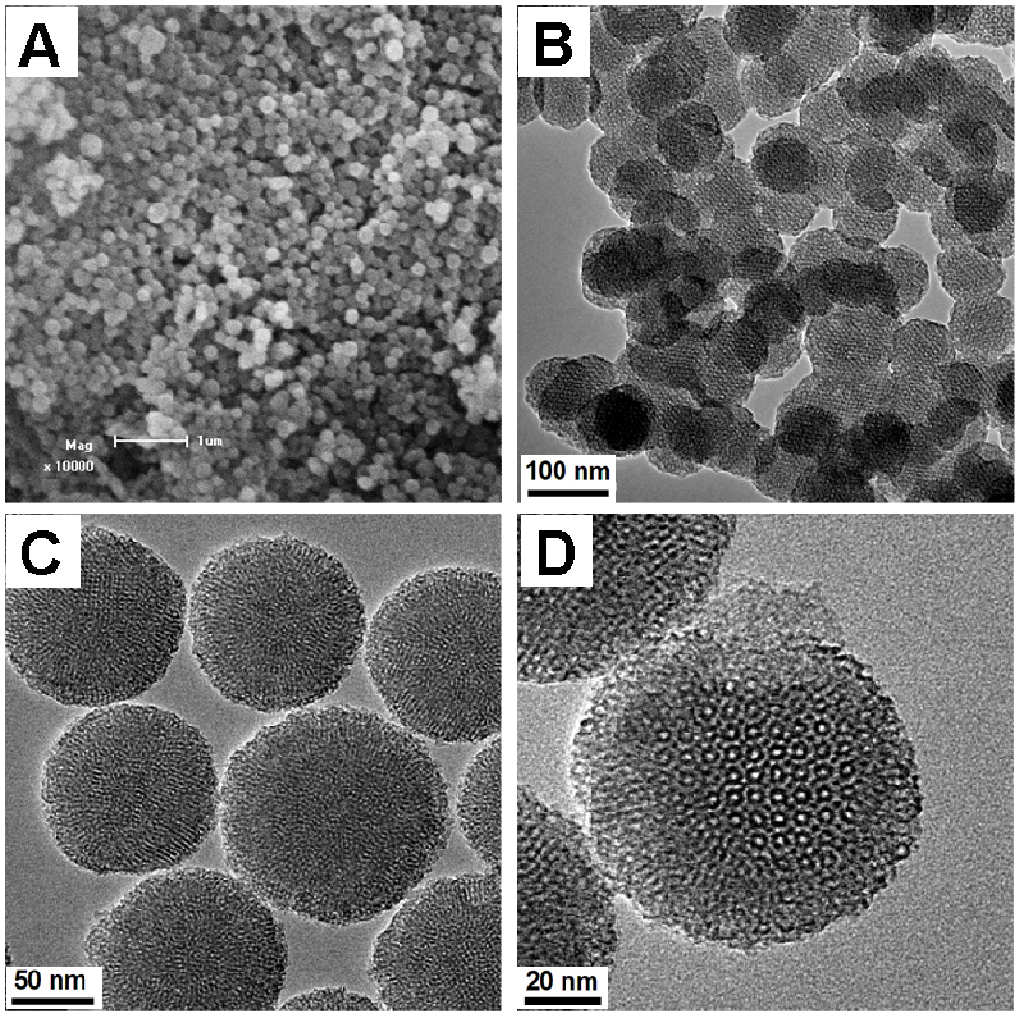

Xu, et al., Fig. 2.

RSC Advances Accepted Manuscript

Scheme 1.

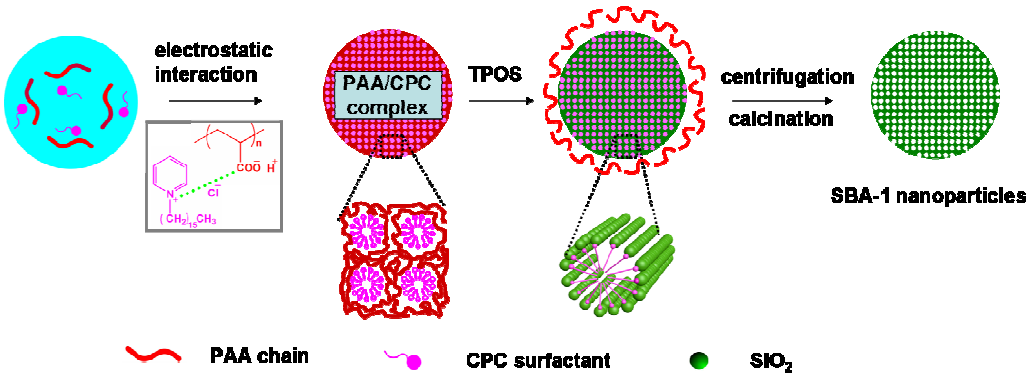

Xu, et al., Scheme 1.

RSC Advances Accepted Manuscript

Fig. 3.

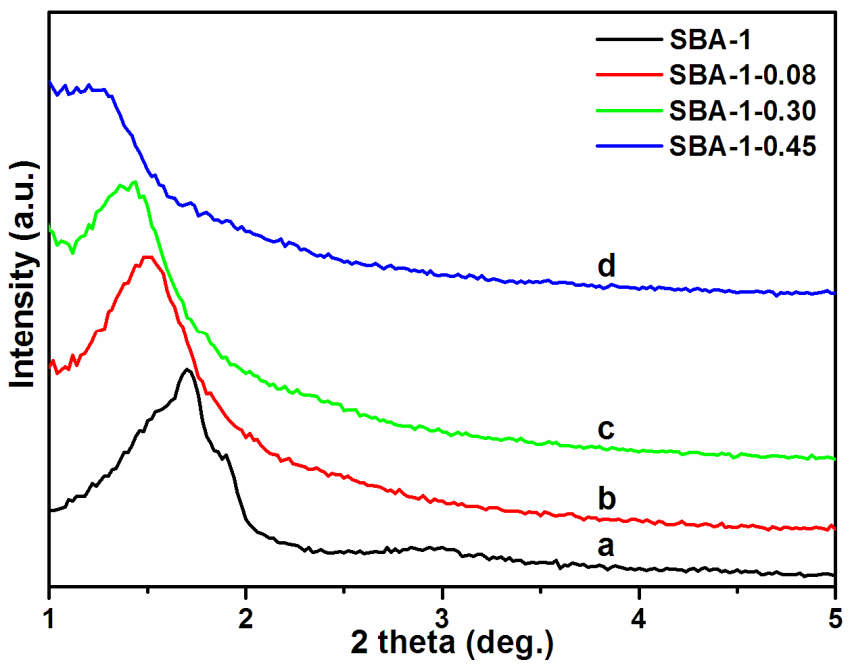

Xu, et al., Fig. 3.

RSC Advances Accepted Manuscript

Fig. 4.

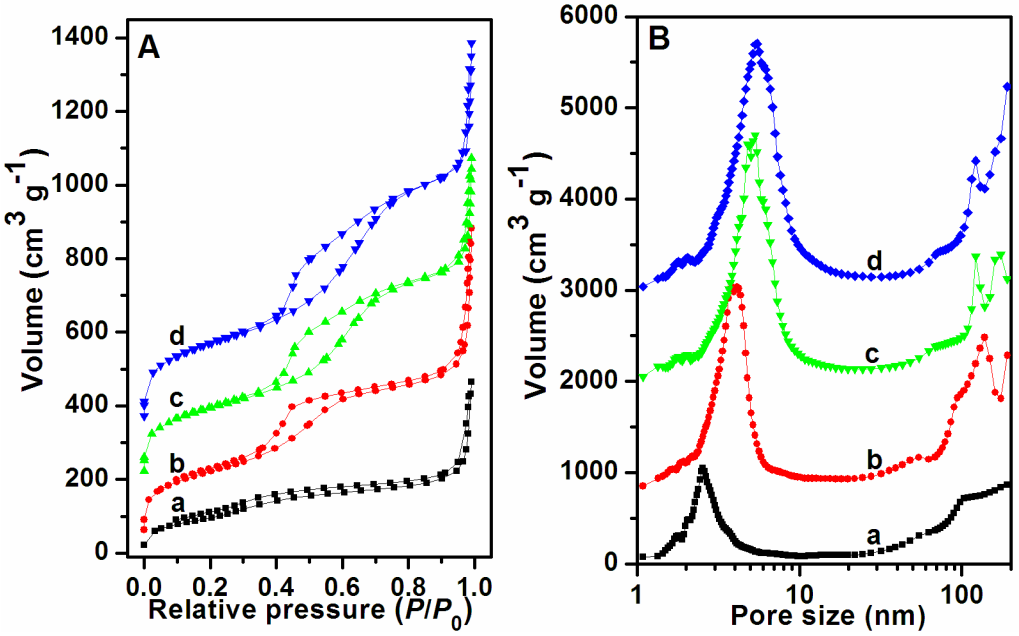

Xu, et al., Fig. 4.

RSC Advances Accepted Manuscript

Fig. 5.

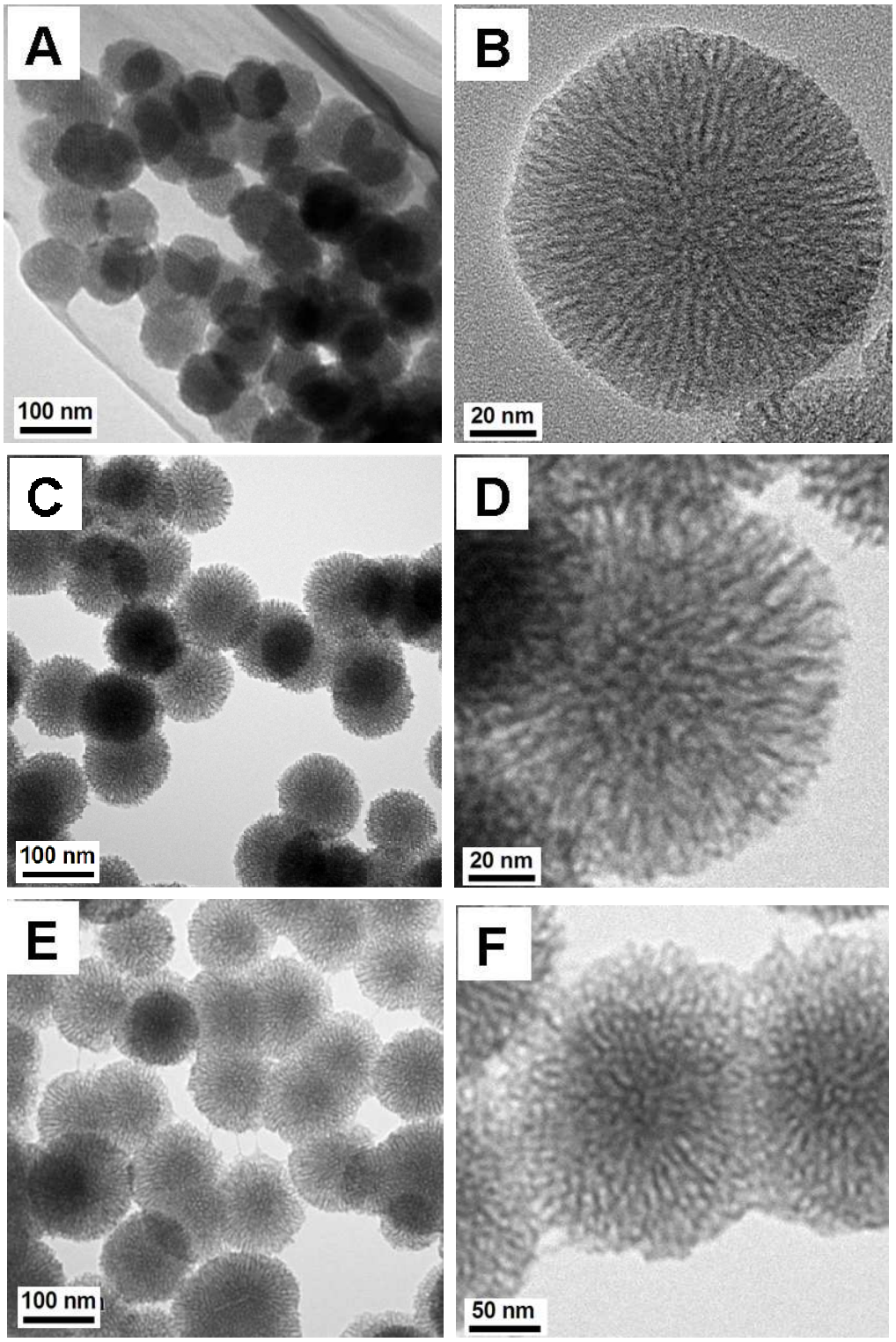

Xu, et al., Fig. 5.

RSC Advances Accepted Manuscript

Fig. 6.

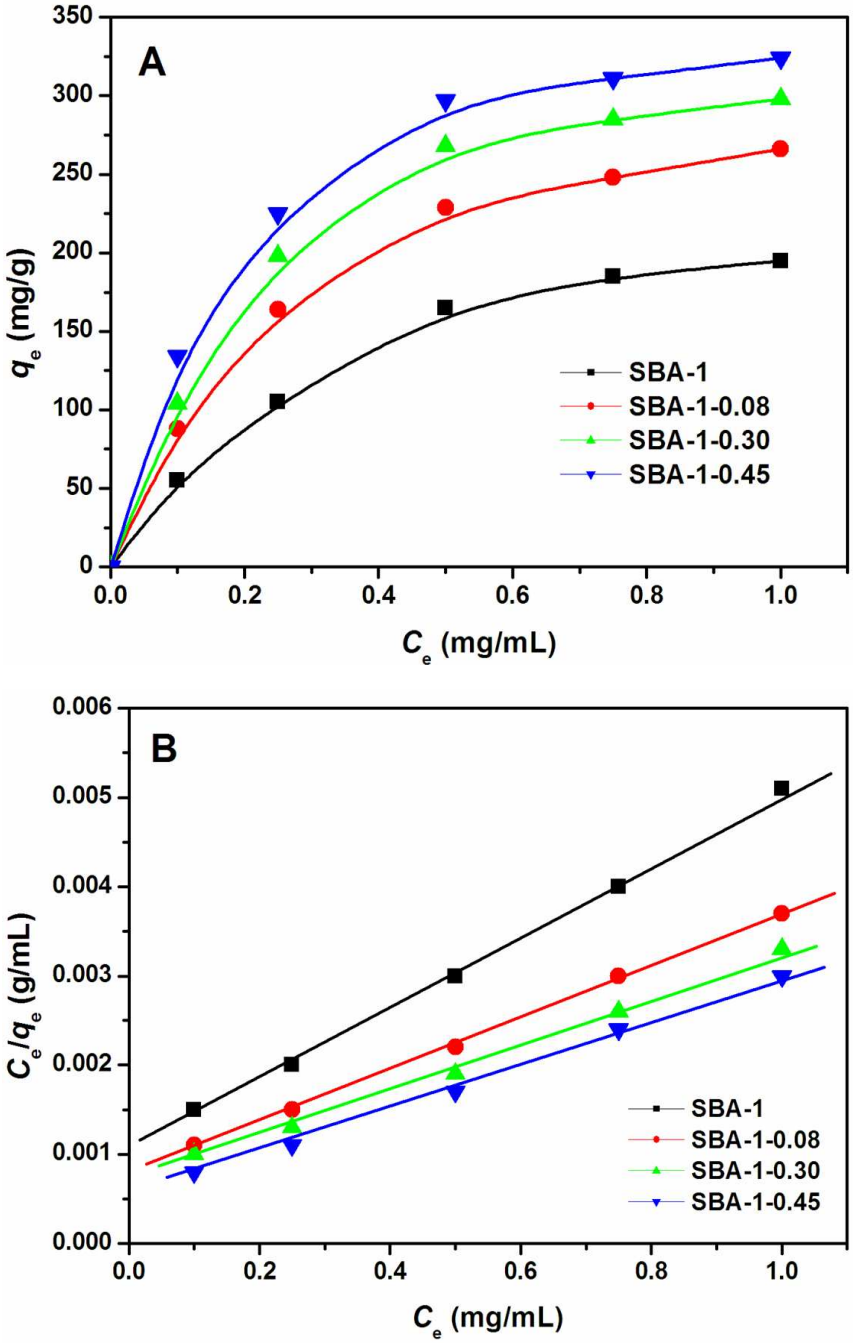

Xu, et al., Fig. 6.

RSC Advances Accepted Manuscript

Fig. 7.

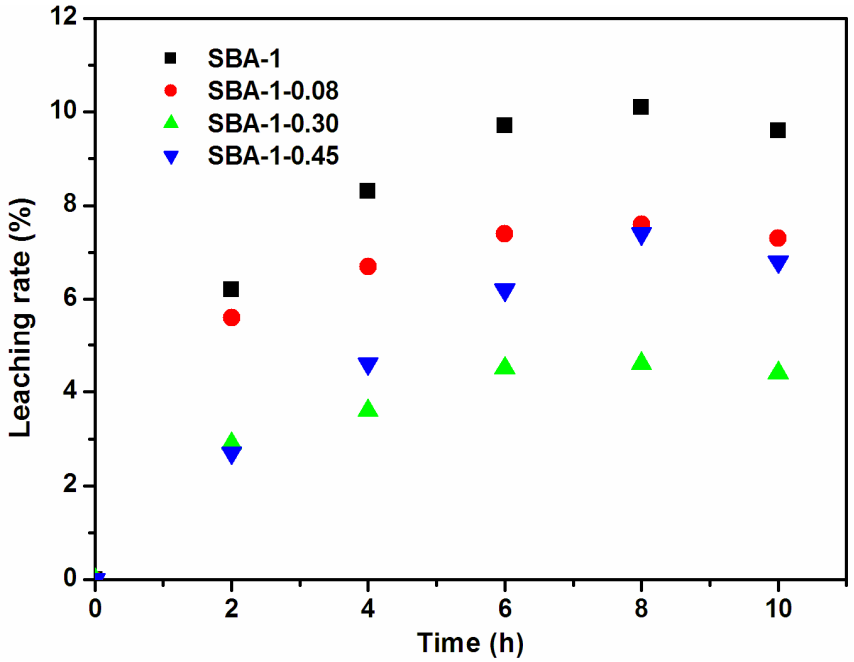

Xu, et al., Fig. 7.

RSC Advances Accepted Manuscript

Fig. 8.

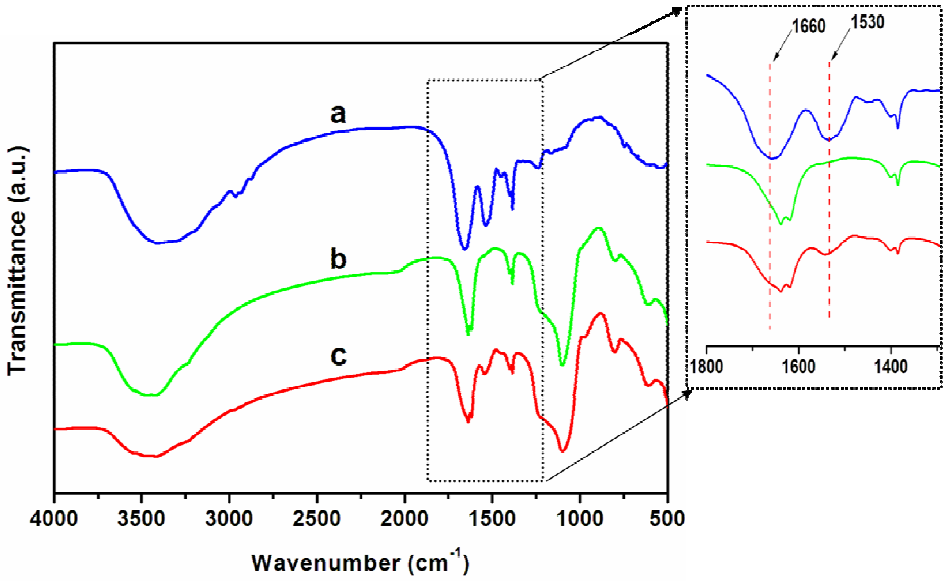

Xu, et al., Fig. 8.

RSC Advances Accepted Manuscript

Table 1.

Sample	Particle size (nm)	Mesopore size (nm)	BET surface area ($m^2 g^{-1}$)	Pore volume ($cm^3 g^{-1}$)	K_L [a] (mL g^{-1})	q_{max} [b] (mg g^{-1})
SBA-1	90	2.5	355	0.80	3.43	250
SBA-1-0.08	100	3.8	662	1.29	3.57	346
SBA-1-0.30	120	4.8	703	1.35	4.12	391
SBA-1-0.45	130	5.3	798	1.60	4.36	409

[a] The adsorption constant for Langmuir adsorption model.

[b] The maximal loading of lysozyme

Xu, et al., Table 1.

RSC Advances Accepted Manuscript

Table 2.

Scaffold	lysozyme bound (mg/g)	Activity (U/mg lysozyme)	Retained activity compared to free enzyme[a] (%)
SBA-1	165	2074	24.0
SBA-1-0.08	229	1458	16.9
SBA-1-0.30	268	872	10.1
SBA-1-0.45	297	766	8.9

[a] Based on the specific activity of free lysozyme at 8640U/mg enzyme.

RSC Advances Accepted Manuscript